Available online at www.sciencedirect.com
SCIENCE DIRECT
Journal of Organometallic Chemistry 691 (2006) 2005–2013
Journal of Organometallic Chemistry
www.elsevier.com/locate/jorganchem

A contribution to the coordination chemistry of 2,3,5,6-tetrakis(α-pyridyl)pyrazine (TPP): Synthesis, spectroscopy, electrochemistry, and density-functional study of {[Mo(CO)$_4$]$_2$(μ-TPP)}

Rodrigo S. Bitzer [a], Robson P. Pereira [a], Ana Maria Rocco [a], José Guilherme S. Lopes [b], Paulo Sérgio Santos [b], Marco A.C. Nascimento [c], Carlos A.L. Filgueiras [a,*]

[a] *Departamento de Química Inorgânica, Instituto de Química, Universidade Federal do Rio de Janeiro, C.P. 68563, Rio de Janeiro, RJ 21945-970, Brazil*
[b] *Laboratório de Espectroscopia Molecular, Instituto de Química, Universidade de São Paulo, Instituto do Milênio de Materiais Complexos, São Paulo, SP 05513-970, Brazil*
[c] *Departamento de Físico-Química, Instituto de Química, Universidade Federal do Rio de Janeiro, Rio de Janeiro, RJ 21949-900, Brazil*

Received 13 October 2005; received in revised form 13 December 2005; accepted 26 December 2005
Available online 21 February 2006

Abstract

The reaction between *cis*-[Mo(CO)$_4$(piperidine)$_2$] and 2,3,5,6-tetrakis(α-pyridyl)pyrazine (TPP) in the 3:1 (Mo:TPP) stoichiometric ratio afforded the organobimetallic compound {[Mo(CO)$_4$]$_2$(μ-TPP)} (**1**) in 89% yield. This complex has been characterized by elemental and thermogravimetric analyses, vibrational (FT-IR and FT-Raman) and electronic spectroscopy, and ^{1}H and ^{13}C-CP/MAS NMR spectroscopy. NMR data have revealed that TPP coordinates to each metal at two adjacent pyridine nitrogen atoms, according to a rare bis-bidentate chelating mode. The cyclic voltammogram of **1** in DMF has shown an irreversible metal-based oxidation at +0.77 V versus SCE. A DFT/B3LYP study of two plausible molecular structures for **1** has been carried out in vacuum using the LACV3P(d,p) and LACV3P++(d,p) basis sets. This theoretical study has pointed to the structure with the Mo(CO)$_4$ moieties on opposite sides with respect to the pyrazine ring (*trans* isomer – C_{2h} symmetry) as the most stable one. The vibrational frequencies of the *trans* structure have been calculated at the B3LYP/LACV3P(d,p) level and compared with the FT-IR and FT-Raman spectra of **1**. An excellent agreement between experimental and calculated frequencies was obtained.

Keywords: Density functional theory; Bimetallic complexes; Molybdenum; Nitrogen heterocyclic ligand; Tetra(α-pyridyl)pyrazine; TPP

1. Introduction

The reactivity and coordinating behavior of 2,3,5,6-tetrakis(α-pyridyl)pyrazine (TPP) toward transition-metal species have been extensively investigated since the late 1980s [1–24]. Moreover, considerable attention has been recently focused on reactions between TPP and polyhalides [25] and on hydrothermal reactions of TPP with inorganic oxides [26], which lead to organic–inorganic hybrid materials. Some of the studies involving TPP and transition metals have shown that this ligand is an effective building block for the construction of oligometallic architectures, which can be prepared, for example, to effect photoinduced electron- and/or energy-transfer processes [5,8,10,18]. Other studies, however, have revealed that TPP exhibits a unique variety of coordination modes [7,12,13]. In fact, no less than seven different chelating modes have so far been reported for TPP. Among them, the bidentate modes (Fig. 1) [12,13,17,20,27] are relatively rare compared to the tridentate modes. Recently, we have succeeded in preparing organotin compounds bearing TPP in the unusual

* Corresponding author. Tel.: +55 21 2562 7812; fax: +55 21 2562 7559.
E-mail address: calf@iq.ufrj.br (C.A.L. Filgueiras).

0022-328X/$ - see front matter © 2006 Elsevier B.V. All rights reserved.
doi:10.1016/j.jorganchem.2005.12.055

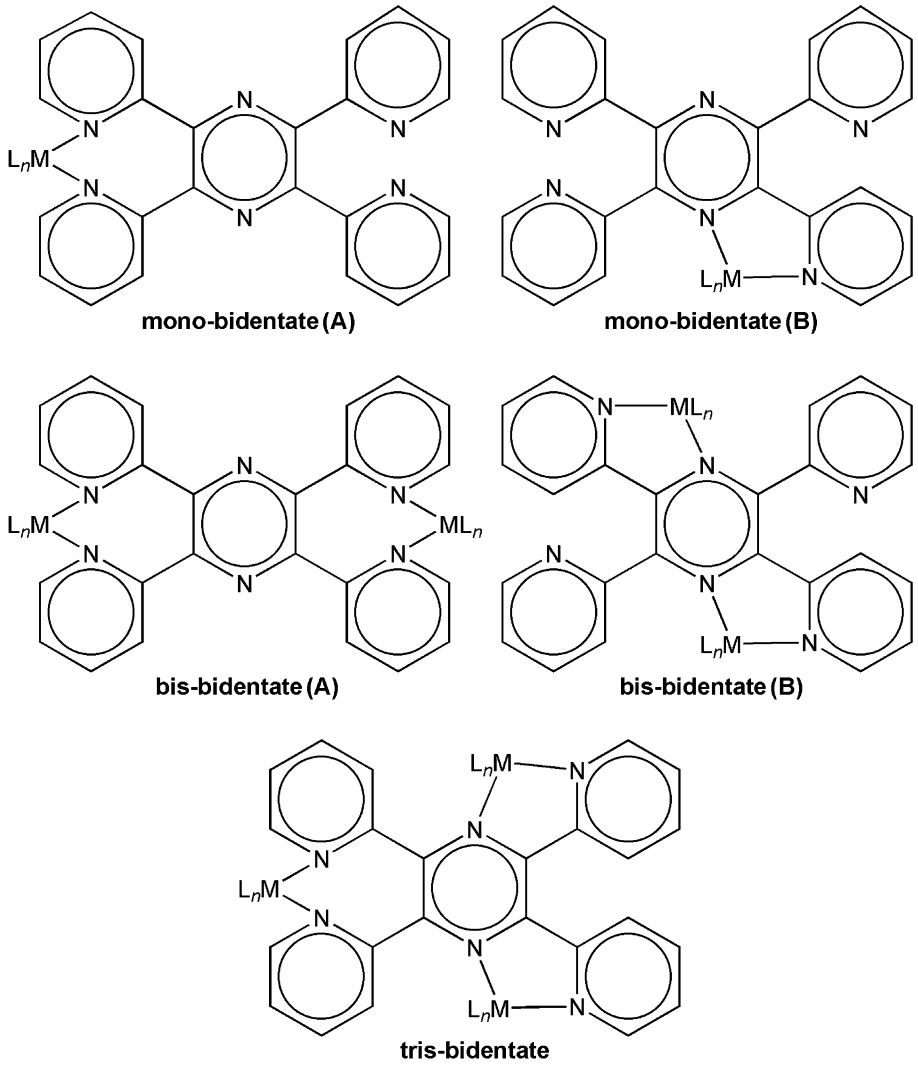

Fig. 1. The bidentate coordination modes of TPP. The mono- and bis-tridentate modes are omitted.

bis-bidentate(A) coordination mode (Fig. 1) [27], and the present work deals with yet another example of this mode.

Reactions involving TPP and organometallic species are relatively scarce. Examples include Re(I) [13], Yb(II) [15], and more recently Ru(II) [17] and Ir(III) [20]. Remarkably, organometallic complexes containing TPP and Group 6 metals have never been described. Therefore, in this article we report the synthesis, spectroscopic and electrochemical characterization, and density functional theory (DFT) study of the first molybdenum carbonyl complex with TPP, namely $\{[Mo(CO)_4]_2(\mu\text{-TPP})\}$ (**1**).

2. Results and discussion

1 was prepared in 89% yield from *cis*-$[Mo(CO)_4(piperidine)_2]$ and TPP in the 3:1 (Mo:TPP) stoichiometric ratio. A large excess of the organometallic reagent (50%) was used to avoid the formation of a mononuclear product. Elemental analysis of **1** (see Section 4) is in agreement with the proposed molecular formula. In addition, the thermogravimetric curve for **1** (Appendix A) shows the loss of the eight carbonyl ligands in the 165–390 °C range. Both the FT-IR and FT-Raman spectra of **1** exhibit four ν(CO) bands (Fig. 2). This result is consistent with the presence of $Mo(CO)_4$ moieties in octahedral environments.

The electronic absorption spectra of pure TPP and of **1** in the 270–800 nm range are shown in Fig. 3. Table 1 summarizes the values of λ_{max} and ε collected from this figure. Regardless of the solvent, **1** exhibits two broad bands in the visible region of the spectra (Fig. 3). These bands are ascribed to metal-to-ligand charge-transfer (MLCT) transitions due to their high ε values (Table 1). The bands at 495 nm (CH_2Cl_2) and at 501 nm (DMF) are assigned to the MLCT Mo → TPP transition, whereas the shoulders at 390 nm (CH_2Cl_2) and at 388 nm (DMF) arise from the lowest-energy MLCT Mo → CO transition (Table 1). These assignments are based on previous studies of complexes of the $[Mo(CO)_4(NN)]$ type (NN = α-diimines or nitrogen heterocyclic ligands) [28]. In the solid-state electronic spectrum of **1** (inset in Fig. 3), the lowest-energy

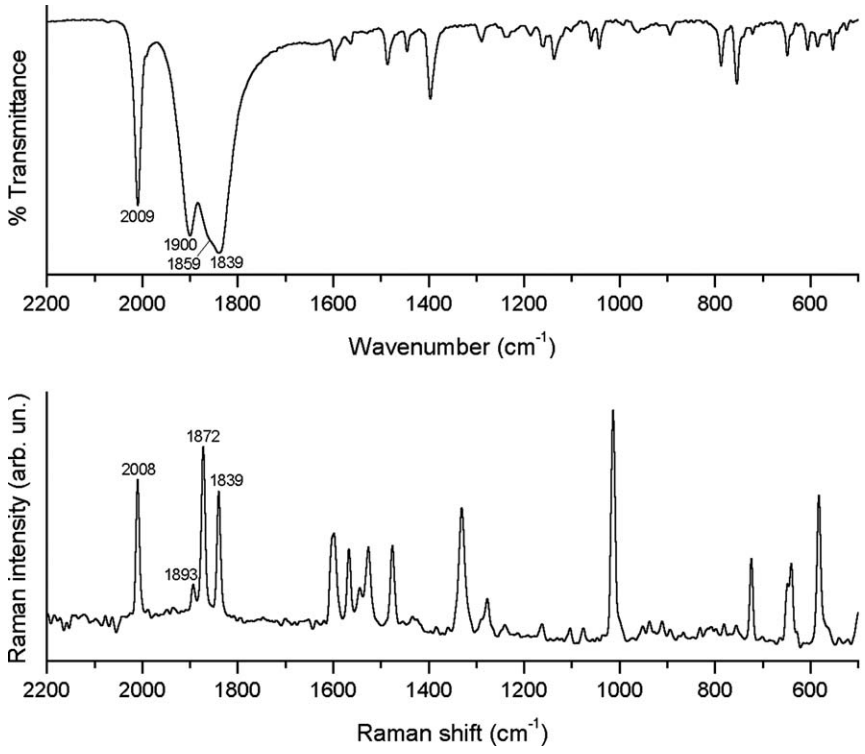

Fig. 2. FT-IR (top) and FT-Raman (bottom) spectra of **1** in the 2200–500 cm^{-1} range.

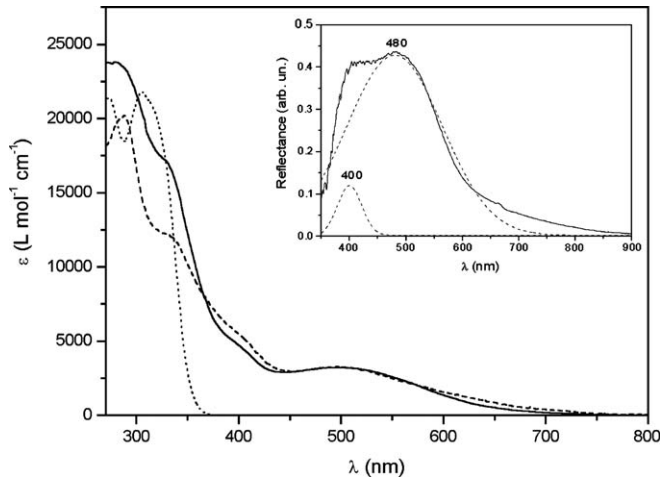

Fig. 3. The electronic absorption spectra of pure TPP (CH_2Cl_2, dotted line) and of **1** (CH_2Cl_2, dashed line; DMF, solid line). Inset: the diffuse reflectance spectrum of **1** (solid line) dispersed in $KClO_4$ (1:25) and its deconvolution (dashed line).

MLCT Mo → CO and MLCT Mo → TPP transitions lie at 400 and 480 nm, respectively. It is worth mentioning that resonance Raman spectra with 514.5 and 632.8 nm excitations were not obtained due to fluorescence exhibited by **1** at these wavelengths.

A striking feature of the electronic absorption spectra of **1** (Fig. 3) is that neither the lowest-energy MLCT Mo → CO nor the MLCT Mo → TPP bands are solvatochromic. Indeed, in complexes of the $[Mo(CO)_4(NN)]$ type, MLCT Mo → CO transitions are not expected to exhibit

Table 1
Electronic spectral data for TPP and for **1**

Compound	Solvent	λ_{max}/nm ($\varepsilon/10^4$ M^{-1} cm^{-1})	Assignment
TPP	CH_2Cl_2	272 (2.2), 305 (2.2), 317sh[a] (2.1)	n → π*, π → π*
1	CH_2Cl_2	288 (2.0), 328 (1.3)	Intraligand
		390sh (0.6)	MLCT Mo → CO
		495 (0.3)	MLCT Mo → TPP
	DMF	322sh (1.8)	Intraligand
		388sh (0.5)	MLCT Mo → CO
		501 (0.3)	MLCT Mo → TPP

[a] sh = shoulder.

solvatochromism; nevertheless, MLCT Mo → NN bands normally bear a high degree of negative solvatochromism [28–30].[1] Furthermore, centrosymmetric dinuclear complexes of the $\{[Mo(CO)_4]_2(\mu\text{-NN})\}$ type (NN = bridging bidentate nitrogen heterocyclic ligand) often exhibit this solvatochromic behavior to an extent greater than that of their mononuclear noncentrosymmetric analogues [29,30]. Thus, it is interesting to note that in **1** the lowest-energy MLCT Mo → TPP band does not bear any degree of negative solvatochromism on going from CH_2Cl_2 to DMF (Table 1). This result suggests that in **1** the difference in molecular polarizability [29], or dipole moment [30], between the ground and the low-lying MLCT Mo → TPP excited states is negligible. To our knowledge, **1** is the first example of an $\{[Mo(CO)_4]_2(\mu\text{-NN})\}$-type complex that

[1] Negative solvatochromism refers to the shift of the MLCT band to lower λ_{max} values as the polarity of the solvent increases.

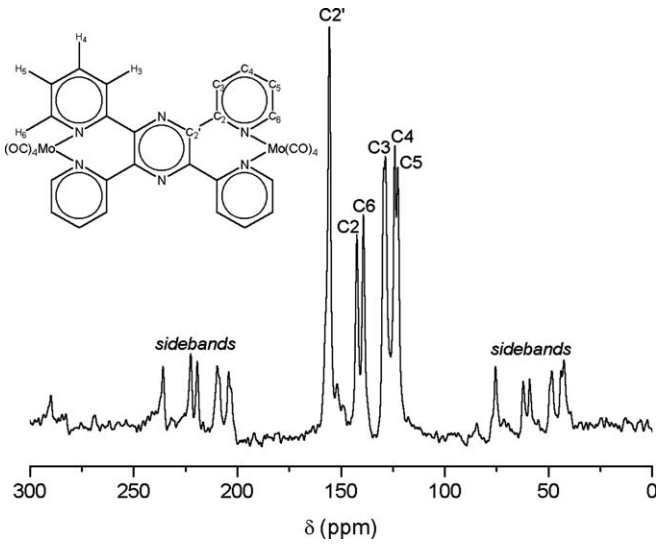

Fig. 4. The ^{13}C-CP/MAS NMR spectrum of **1**. Spectrum recorded at a rotational frequency of 6 kHz.

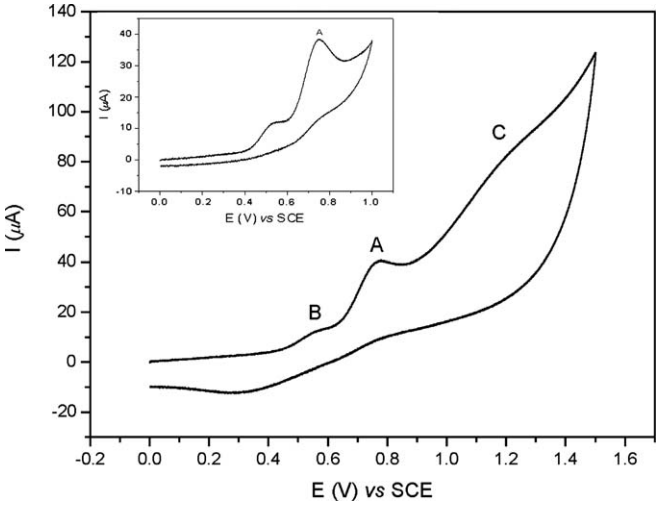

Fig. 5. The cyclic voltammogram (CV) of **1** in DMF in the region from 0.0 to +1.5 V vs. SCE. Inset: CV from 0.0 to +1.0 V vs. SCE showing the irreversibility of process A. Peak A is assigned to a molybdenum-localized oxidation, and peaks B and C arise due to decomposition products.

does not exhibit the negative solvatochromic behavior of the lowest-energy MLCT Mo → NN band.

The NMR data for **1** indicate that each molybdenum atom is bound to two adjacent pyridine nitrogen atoms of TPP. The number and integration of the ^{1}H signals in solution (DMF-d_7 or $CDCl_3$) (see Section 4) and the number of the isotropic ^{13}C signals in the solid-state spectrum (Fig. 4) imply that no uncoordinated pyridine ring exists in **1**. Hence, according to the solution and the solid-state NMR data, of the two bis-bidentate chelating modes of TPP (Fig. 1), only the bis-bidentate(A) mode can occur in **1**. Attempts to observe the ^{13}CO signals in the ^{13}C-CP/MAS NMR spectrum of **1** (Fig. 4) were unsuccessful due to the low sensitivity of these signals. The ^{1}H and ^{13}C NMR data of pure TPP are supplied for comparison in Appendix A.

The electrochemical oxidation of **1** in DMF has been investigated by cyclic voltammetry. The cyclic voltammogram of **1** (Fig. 5) exhibits an electrochemically irreversible metal-centered oxidation at +0.77 V versus SCE. Electrochemical oxidation of complexes of both $[Mo(CO)_4(NN)]$ and $\{[Mo(CO)_4]_2(\mu\text{-NN})\}$ types normally occurs in a single irreversible step [28]. The same is observed for **1**.

According to the NMR data, **1** has TPP as a bis-bidentate(A) chelating ligand. Thus, two plausible molecular structures can be proposed for **1** (Fig. 6): (i) a *trans* isomer – structure (**1t**) containing the $Mo(CO)_4$ moieties on opposite sides with respect to the pyrazine ring (C_{2h} symmetry); (ii) a *cis* isomer – structure (**1c**) with the $Mo(CO)_4$ moieties on the same side with relation to the pyrazine ring (C_2 symmetry). The latter (*cis* isomer) was first observed in the cation $\{[Pt(PEt_3)Cl]_2(\mu\text{-TPP})\}^{2+}$ [12], and the former (*trans* isomer) has never been reported. Optimization of these two possible structures for **1** has been performed in the gas phase at the DFT level of calculation, using the

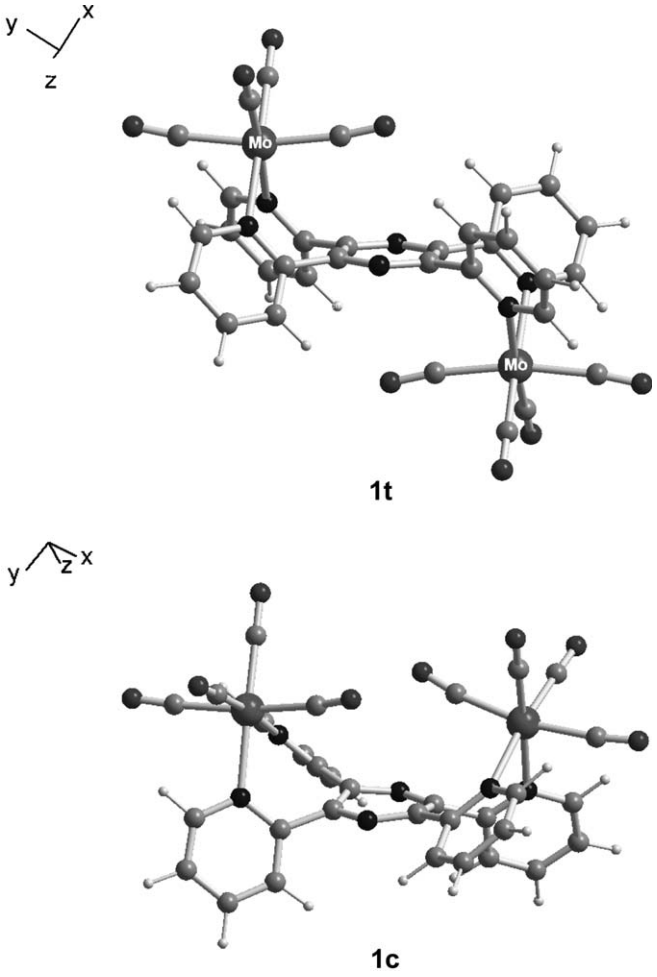

Fig. 6. Structures of the *trans* (**1t**) and the *cis* (**1c**) isomers of **1** optimized at the B3LYP/LACV3P++(d,p) level.

B3LYP hybrid functional along with the LACV3P(d,p) and LACV3P++(d,p) basis sets (see Section 4.4). Fig. 6 illustrates the molecular structures optimized for the *trans* (**1t**) and the *cis* (**1c**) isomers of **1** at the B3LYP/LACV3P++(d,p) level. The total relative energies (ΔE_T) calculated for **1t** and **1c** are given in Table 2. Table 3 shows selected geometric parameters calculated for **1t** (the most stable isomer) and **1c**.

Regardless of the basis set used, Table 2 shows that **1t** is favored over **1c** by more than 9 kcal mol^{-1}. Structure **1c** is the least stable one due to the steric repulsion between the axial carbonyl groups oriented toward the pyrazine ring. This repulsive interaction gives rise to a considerable distortion of the pyrazine ring of **1c**, which can be measured by the θ[N_{pz}–C2′–C2′–N_{pz}] dihedral angle, equal to 15° (Table 3). The atom numbering in Table 3 is the same as that given in Fig. 4.

The geometric parameters for **1t** listed in Table 3 are quite reasonable and in accordance with previous DFT and X-ray crystallographic studies of other $Mo(CO)_4$-containing compounds [28]. For **1c**, however, owing to its distorted structure, some anomalies in the calculated geometric parameters can be found. For instance, for each $Mo(CO)_4(NN)$ moiety, within a given basis set, the Mo–N bond distances are different from each other (Table 3). The same occurs for the Mo–C_{eq} bond lengths and the Mo–C–O_{eq} bond angles. According to Table 3, inclusion of diffuse functions into the basis set does not lead to relevant changes in the geometric parameters. For **1t**, the structural parameters related to the axial Mo–CO moiety oriented toward the central ring do not significantly differ from those associated with the other axial Mo–CO moiety. This behavior was not observed for **1c**. Table 3 also shows that, regardless of the basis set and isomer, the N_{py}–Mo–N_{py} bite angle is ca. 80°, and the axial C–Mo–C moiety is bent away from TPP by ca. 169°. Also, the equatorial C–Mo–C angle is very close to 90°. These theoretical values resemble those experimental values (determined by single-crystal X-ray diffraction) obtained for [$Mo(CO)_4(NN)$]-type complexes in which the molybdenum atoms form stable five-membered rings [28]. Therefore, in spite of forming a non-planar seven-membered metalacycle (see Fig. 6), according to the DFT results, each molybdenum atom in **1** exhibits a coordination geometry very close to that found in other $Mo(CO)_4$-containing compounds bearing planar five-membered metalacycles.

Table 2
Relative energies (ΔE_T, kcal mol^{-1}) and dipole moments (μ_D, D) calculated for **1t** and **1c**

	ΔE_T	μ_D
B3LYP/LACV3P(d,p)[a]		
1t[b]	0.00	0.11
1c	9.39	17.8
B3LYP/LACV3P++(d,p)		
1t[c]	0.00	0.11
1c	9.71	17.8

[a] Regarding the zero-point energy, the ΔE_T (**1c**) value is 9.26 kcal mol^{-1}.
[b] The absolute total energy for **1t** is −2295.197603 hartree.
[c] The absolute total energy for **1t** is −2295.225899 hartree.

Table 3
Selected geometric parameters calculated for **1t** and **1c**[a,b]

	1t		**1c**	
	B3LYP/LACV3P(d,p)	B3LYP/LACV3P++(d,p)	B3LYP/LACV3P(d,p)	B3LYP/LACV3P++(d,p)
Bond lengths (Å)				
Mo–N_{py}	2.367	2.366	2.330 and 2.400	2.329 and 2.400
Mo–C_{eq}	1.994	1.992	1.985 and 1.999	1.985 and 1.999
Mo–C_{ax1}[c]	2.055	2.055	2.070	2.071
Mo–C_{ax}	2.063	2.063	2.050	2.052
C–O_{eq}	1.156	1.157	1.156	1.156
C–O_{ax1}[c]	1.155	1.154	1.147	1.148
C–O_{ax}	1.152	1.152	1.154	1.154
Bond angles (°)				
N_{py}–Mo–N_{py}	79.4	79.5	80.0	81.2
C_{eq}–Mo–C_{eq}	91.0	90.9	90.5	90.7
C_{ax}–Mo–C_{ax1}	169.8	169.3	168.5	168.3
Mo–C–O_{eq}	178.8	178.9	179.0 and 178.7	179.0 and 178.7
Mo–C–O_{ax1}	173.5	172.8	171.0	170.8
Mo–C–O_{ax}	173.9	173.6	174.1	173.7
Dihedral angles (°)				
N_{pz}–C2′–C2′–N_{pz}	0.2	0.0	15.3	15.4
N_{pz}–C2′–C2–N_{py}	+122.3 and −122.3	+122.3 and −122.3	+118.0 and −140.7	+118.0 and −140.7

[a] Bond lengths are given in Å and angles in °.
[b] ax and eq stand for axial and equatorial, respectively; py and pz stand for pyridine and pyrazine rings, respectively.
[c] C_{ax1} and O_{ax1} stand for the axial CO group oriented toward the pyrazine ring.

The DFT calculations have pointed to the *trans* structure as the most stable form of **1** in the gas phase (Table 2). There is no reason, however, for discarding the same preference in solution and in the solid state. The steric repulsion between the axial CO groups oriented toward the pyrazine ring in the *cis* isomer (**1c** in Fig. 6) plays a major role in destabilizing this structure. Such an intramolecular repulsive interaction will be operative regardless of the medium. Therefore, the *trans* isomer (**1t** in Fig. 6), which does not exhibit any repulsive interaction between axial CO groups, is likely to be the favored form of **1** not only in vacuum, but also in solution and in the solid state. Supporting evidence for the *trans* structure in the solid state can be found not only by comparison between the FT-IR and FT-Raman spectra of **1**, but also by comparing the vibrational frequencies calculated for **1t** at the B3LYP/LACV3P(d,p) level with the experimental bands of **1**.

The vibrational frequencies of the optimized *cis* (C_2 symmetry) and *trans* (C_{2h} symmetry) geometries were calculated at the B3LYP/LACV3P(d,p) level. No imaginary frequencies were found, indicating that both structures are minima in the potential energy surface of **1**. For the C_2 symmetry, all normal vibration modes are both IR and Raman active. However, for molecules falling into the C_{2h} point group, according to the mutual exclusion rule, IR-active (A_u and B_u) bands have irreducible representations different from those of the Raman-active (A_g and B_g) bands. This marked difference between the vibrational spectra calculated for the *cis* and *trans* isomers can be reliably used for studying the structure of **1**.

The FT-IR and FT-Raman spectra of **1** in the region below 1700 cm^{-1} are depicted in Fig. 7. Table 4 summarizes the results of the vibrational analysis of **1**, which has been carried out by comparing the bands observed for **1** with the frequencies calculated for the *trans* isomer (**1t**) at the DFT level of calculation. An excellent agreement between experimental and calculated frequencies was obtained, except for the ν(CO) bands; nevertheless, the discrepancies between the calculated and the observed ν(CO) bands are acceptable [31]. It is important to mention that a comparison between the frequencies calculated for the *cis* isomer (**1c**) and those observed for **1** was made but the result was not satisfactory. In Table 4, only the high-frequency bands showing accidental degeneracy are listed. In the low-frequency region (below 650 cm^{-1}), however, a more comprehensive analysis is made since a reliable assignment in this region is only possible with the aid of high-level quantum-chemical calculations. The presence of the carbonyl stretches and the motions of the TPP rings mainly characterize the high-frequency region of the vibrational spectrum of **1**. The region below 650 cm^{-1}, in turn, is characterized by the presence of bending and stretching modes of the organometallic moieties. These metal–ligand vibrations often occur strongly coupled to TPP internal vibrations.

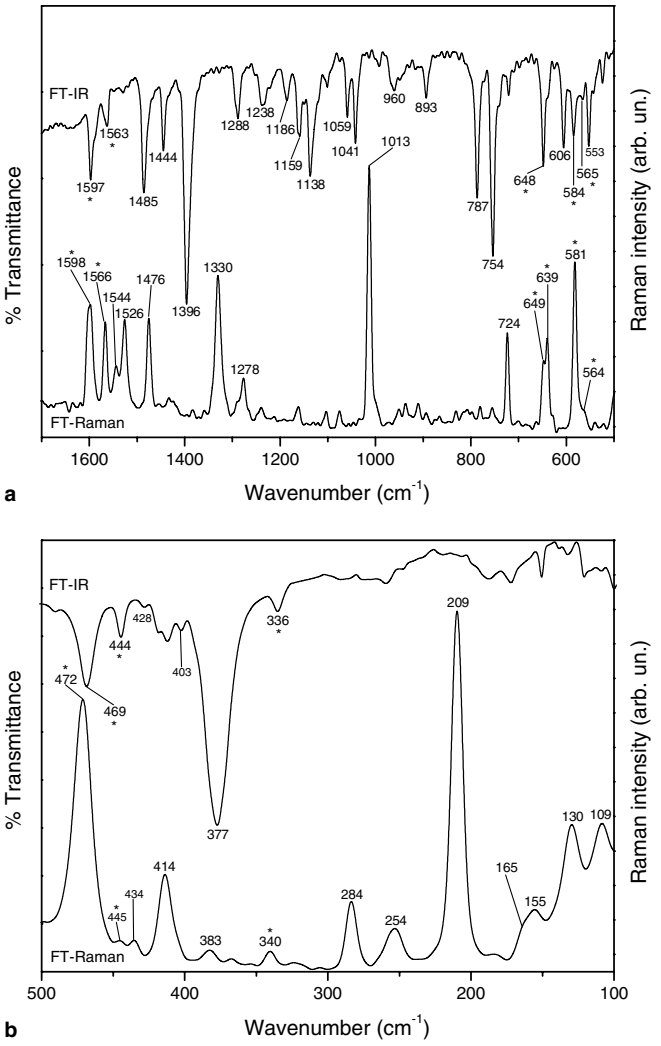

Fig. 7. FT-IR and FT-Raman spectra of **1** in the 1700–500 cm^{-1} (a) and 500–100 cm^{-1} (b) ranges. Asterisks indicate the accidentally coincidental bands.

Figs. 2 (carbonyl region) and 7 show that some IR and Raman bands of **1** exhibit essentially the same frequencies. However, the DFT calculations of the normal vibration modes of **1t** have revealed that these coincidences are accidental, that is, despite having the same frequencies, the bands have different representations (or species) (Table 4). The presence of accidental degeneracy in centrosymmetric molecules has already been discussed in the literature [32]. In **1**, the accidental coincidences can be thought of as resulting from the fact that the vibrational modes are localized on the individual heterocyclic rings and organometallic moieties, and the interaction (electronic communication) between the pyridine rings across the pyrazine ring is very small. In summary, even though the FT-IR and FT-Raman spectra of **1** exhibit some coincidental bands (Figs. 2 and 7), these coincidences are accidental owing to the lack of electronic communication between the $Mo(CO)_4$ moieties. Therefore, in view of the results shown in Table 4, it is possible to conclude that **1** is likely to occur as the *trans* isomer in the solid state.

Table 4
Vibrational analysis of **1**[a]

IR	Raman	Calculated for **1t** [B3LYP/LACV3P(d,p)]	Assignment[b,c,d] (prevailing character)	Species[e]
2009	2008	2077.1	$\nu^{s}_{CO(ax)} + \nu^{s}_{CO(eq)}$	A_g
		2075.5	$\nu^{s}_{CO(ax)} + \nu^{s}_{CO(eq)}$	B_u
1900	1893[f]	1989.9	$\nu^{s}_{CO(ax)}$[g] $+ \nu^{s}_{CO(eq)}$	B_u
1859	1872	1962.1	$\nu^{as}_{CO(ax)}$	B_u
		1961.4	$\nu^{as}_{CO(ax)}$	A_g
1839	1839	1975.9	$\nu^{as}_{CO(eq)}$	A_u
		1974.7	$\nu^{as}_{CO(eq)}$	B_g
1597	1598	1607.1	$\nu_{CC+CN(py)}$	A_g
		1605.4	$\nu_{CC+CN(py)}$	A_u
		1605.1	$\nu_{CC+CN(py)}$	B_g
		1604.3	$\nu_{CC+CN(py)}$	B_u
1563	1566	1562.8	$\nu_{CC(pz)}$	A_g
		1562.8	$\nu_{CC(pz)}$	B_u
648	649	651.7	$\delta^{S}_{C–Mo–C(ax+eq)}$	A_g
		650.4	$\delta^{S}_{C–Mo–C(ax+eq)}$	B_u
		648.9	Intraligand[h]	A_g
		648.2	Intraligand	A_u
		647.4	Intraligand	B_g
[i]	639	641.3	Intraligand	B_g
606	[i]	606.1	$\delta^{W}_{C–Mo–C(eq)}$	B_u
		600.7	$\delta^{W}_{C–Mo–C(ax)}$	A_u
584	581	590.0	Intraligand	B_g
		572.5	Intraligand	B_u
565[f]	564	569.9	$\delta^{T}_{C–Mo–C(eq)}$	A_u
		569.9	$\delta^{T}_{C–Mo–C(eq)}$	B_g
		569.6	$\delta^{S}_{C–Mo–C(ax+eq)}$	A_g
		568.8	$\delta^{S}_{C–Mo–C(ax+eq)}$ + intraligand	B_u
553	[i]	553.4	Intraligand	B_u
469[j]	472[j]	490.0	$\delta^{R}_{C–Mo–C(eq)}$	B_g
		488.6	$\delta^{R}_{C–Mo–C(eq)}$	A_u
		460.6	Intraligand	B_u
		457.1	Intraligand	B_g
		452.9	$\nu^{s}_{Mo–C(eq)}$	A_g
		452.1	$\nu^{s}_{Mo–C(eq)}$	B_u
444	445	448.7	$\nu^{as}_{Mo–C(eq)}$	A_u
		448.5	$\nu^{as}_{Mo–C(eq)}$	B_g
428	[i]	430.0	Intraligand	A_u
[i]	414[j]	424.2	Intraligand	B_g
		403.9	$\nu^{s}_{Mo–C(ax)}$	A_g
		397.1	$\delta^{R}_{C–Mo–C(ax)}$	A_g
403	[i]	403.8	$\nu^{s}_{Mo–C(ax)}$	B_u
[i]	383[j]	382.6	$\delta^{T}_{C–Mo–C(ax)}$	B_g
		376.2	$\nu^{as}_{Mo–C(ax)}$	A_g
377[j]	[i]	398.1	$\delta^{R}_{C–Mo–C(ax)}$	B_u
		392.5	Intraligand	A_u
		383.6	$\delta^{T}_{C–Mo–C(ax)}$	A_u
		376.0	$\nu^{as}_{Mo–C(ax)}$	B_u
336	340	341.8	Intraligand	B_g
		334.8	Intraligand	B_u
[i]	284	280.1	$\delta^{W}_{N–Mo–N}$	A_g
[i]	254[j]	249.9	$\delta^{S}_{N–Mo–N}$	A_g
		241.6	Intraligand	B_g
[i]	209	213.9	$\delta^{R}_{N–Mo–N}$	B_g
		195.8	$\nu^{s}_{Mo–N}$	A_g

[a] Frequencies in cm^{-1}.
[b] ν, stretching modes (s, symmetric or as, antisymmetric); δ, bending modes.
[c] Bending modes: δ^{R}, *in-plane* rocking; δ^{S}, *in-plane* scissoring; δ^{W}, *out-of-plane* wagging; δ^{T}, *out-of-plane* twisting.
[d] ax and eq stand for axial and equatorial, respectively; py and pz stand for pyridine and pyrazine rings, respectively.
[e] The assignment is based on an overall C_{2h} symmetry. A_g and B_g modes are Raman active, and the A_u and B_u modes are IR active.
[f] Very weak.
[g] This mode does not involve the axial CO groups oriented toward the pz ring.
[h] The bands designed as intraligand involve internal TPP modes not uniquely attributable.
[i] Not observed.
[j] Very broad.

3. Conclusions

The bimetallic complex {[$Mo(CO)_4$]$_2$(μ-TPP)} (**1**) was prepared and characterized by different spectroscopic techniques, which revealed that each molybdenum atom is bound to two adjacent pyridine nitrogen atoms of TPP. DFT/B3LYP calculations were performed in order to investigate the molecular structure of **1**. These calculations are consistent with the *trans* isomer (**1t** in Fig. 6) being the most stable form of **1**.

4. Experimental

4.1. General details

Reagents (Strem or Acros) and solvents (Vetec) were obtained from commercial sources. The solvents used in the electronic absorption spectra (CH_2Cl_2 and DMF) and electrochemical measurements (DMF) were previously dried over activated 3 Å molecular sieves (Merck). DMF-d_7 and $CDCl_3$ (Cambridge Isotopes) were stored over activated 3 Å molecular sieves. The reaction was carried out under argon using Schlenk-type glassware and vacuum/inert-gas line manipulation techniques. The work-up of the reaction mixture was done in air. TPP [33] and *cis*-[$Mo(CO)_4$(piperidine)$_2$] [34] were prepared according to the literature. CH_2Cl_2 was dried (CaH_2) and deoxygenated according to standard procedures.

4.2. Physical measurements

Elemental analysis (C, H, and N) was conducted on a Perkin–Elmer 2400 CHN Elemental Analyzer. Thermogravimetric analysis (TGA) was performed under N_2 in the 20–900 °C range on a Perkin–Elmer TGA 7 instrument using a scanning rate of 5.0 °C min^{-1}. IR spectra were recorded on a Magna-IR760 FT-IR Nicolet spectrometer. The spectra were obtained using either KBr pellets (4000–400 cm^{-1}) or Nujol mull in polyethylene (500–50 cm^{-1}), and a resolution of 4 cm^{-1}. Raman spectra with 1064 nm excitation from a Nd^{3+}/YAG laser were registered in the solid state using a Bruker RFS 100/S spectrometer equipped with a germanium detector cooled at liquid N_2 temperature. The spectra were collected up to 8192 spectral accumulations over the 3500–100 cm^{-1} range using a resolution of 4 cm^{-1}, and the laser power was kept at 15 mW. Electronic absorption spectra in solution (CH_2Cl_2 and DMF) were measured at room temperature (r.t.) using a Varian Cary 1E UV–Vis spectrophotometer. The solid-state electronic spectrum of **1** dispersed in $KClO_4$ (1:25) was recorded at r.t. using the diffuse reflectance technique on a Guided Wave 260 instrument equipped with a fiber-optic Wand probe and with silicon and germanium detectors. The ^1H (DMF-d_7 or $CDCl_3$) and ^{13}C-CP/MAS NMR spectra were acquired from a Bruker DRX300 instrument operating at 300.00 MHz (^1H) and at 75.47 MHz (^{13}C). All NMR studies were performed at 293 K, and the chemical shift (δ, ppm) values were determined in relation to $SiMe_4$. In the ^{13}C-CP/MAS NMR spectra the samples were spun at 6–8 kHz in 7 mm diameter zirconia rotors with Kel-f caps. All spectra were obtained using simple pulse sequence (Bloch decay). The ^{13}C-CP/MAS NMR spectrum of **1** was measured using a contact time of 1 ms and a relaxing delay of 20 s. For TPP (Appendix A), the ^{13}C-CP/MAS NMR spectrum was obtained with a contact time of 0.5 ms and a relaxing delay of 60 s. Electrochemical measurements were performed at r.t. using an Autolab EcoChimie PGSTAT 30 instrument, which does not require the use of internal references. The cyclic voltammograms were obtained under argon from electrochemical cells equipped with a working electrode of Pt disk ($\varnothing = 3$ mm), a saturated calomel (SCE) reference electrode without regard for liquid junction potentials, and with a Pt sheet (2 cm^2) as counter electrode. The cyclic voltammograms were measured from DMF (ca. 10^{-3} M) solutions with ca. 0.1 M Bu_4NClO_4 as supporting electrolyte. A sweep rate of 50 mV s^{-1} was employed in all experiments.

4.3. Synthesis of {[Mo(CO)$_4$]$_2$(μ-TPP)} (1)

Solid TPP (285 mg, 0.7 mmol) was slowly added under vigorous magnetic stirring to a yellow suspension of *cis*-[$Mo(CO)_4$(piperidine)$_2$] (836 mg, 2.2 mmol) in CH_2Cl_2 (40 mL). The reaction mixture was stirred at r.t. in the dark for 108 h. After this period, the resulting red precipitate (**1**) was isolated by filtration, washed with hot CH_2Cl_2 (5 × 15 mL), and dried under vacuum. Yield: 500 mg (89%). M.p.: 165 °C (d). Anal. Calc. for $C_{32}H_{16}N_6O_8Mo_2$: C, 47.78; H, 2.00; N, 10.45. Found: C, 47.22; H, 1.98; N, 10.44%. FT-IR (cm^{-1}, KBr pellet): ν(CO), 2009(s), 1900(s), 1859(sh), 1838(vs,br); ν(CC + CN), 1597(m), 1563(w), 1485(m), 1444(w), 1396(m); δ(CH), 787(m), 757(m), 753(sh). FT-Raman (cm^{-1}, $\lambda = 1064$ nm): ν(CO), 2008(s), 1893(vw), 1872(vs), 1839(s); ν(CC + CN), 1598(m), 1566(w), 1544(w), 1526(m), 1476(m), 1330(m); δ(CH), 724(m). ^1H NMR (DMF-d_7 or $CDCl_3$, 300.0 MHz, 293 K): δ (ppm), 7.42 (m, 1H, H5), 8.03 (m, 1H, H4), 8.17 (m, 1 H, H3), 8.36 (d, $J_{HH} = 4.4$ Hz, 1 H, H6). In DMF-d_7, the signal for H4 was not observed due to the solvent signal [δ 8.01 (m,br)]. ^{13}C-CP/MAS NMR (75.5 MHz, 293 K): δ (ppm), 122.5 (C5), 124.0 (C4), 129.4 (C3), 139.1 (C6), 142.3 (C2), 155.5 (C2′-pyrazine ring). The atom numbering is that shown in Fig. 4. Due to the low solubility of **1** in common organic solvents and decomposition within a few hours in DMF and DMSO, its $^{13}C\{^1H\}$ NMR spectrum in solution could not be measured. Attempts to grow suitable single crystals of **1** for X-ray diffraction were unsuccessful.

4.4. Computational details

All geometry optimizations were carried out in vacuum using the JAGUAR 5.5 program [35] with an energy convergence criterion of 5.00×10^{-8} hartree. The calculations

were performed using the DFT method with the hybrid exchange-correlation functional B3LYP [36] and with the LACV3P(d,p) [6-311G(d,p) for C, H, N, and O, and Los Alamos ECP [37] plus valence double-ζ for Mo] and LACV3P++(d,p) [6-311++G(d,p) for C, H, N, and O, and Los Alamos ECP plus valence double-ζ for Mo] basis sets. No symmetry or geometry constraints were imposed in the calculations. The vibrational frequencies of each geometry optimized at the B3LYP/LACV3P(d,p) level were analytically determined at the same level of calculation and verified to be real. The use of scaling factors for the calculated frequencies was not required at this level of calculation. Of the many available functionals, we have chosen B3LYP because it has provided accurate results for organic molecules in general and for Group 6 metal–carbonyl complexes containing *N*-donor ligands [28].

Acknowledgements

The authors thank CAPES, CNPq, FAPERJ, FUJB, and CT-Energ/FINEP/PETROBRÁS for sponsorship. The authors also acknowledge Prof. Rosane A.S.S. Gil (IQ-UFRJ) for the ^{13}C-CP/MAS NMR spectra and Prof. Judith Felcman (PUC-RJ) for the thermogravimetric analysis.

Appendix A. Supplementary data

Supplementary data associated with this article can be found, in the online version, at doi:10.1016/j.jorganchem.2005.12.055.

References

[1] R.P. Thummel, S. Chirayil, Inorg. Chim. Acta 154 (1988) 77.
[2] R. Ruminski, J. Kiplinger, T. Cockroft, C. Chase, Inorg. Chem. 28 (1989) 370.
[3] R.R. Ruminski, C. Letner, Inorg. Chim. Acta 162 (1989) 175.
[4] R.R. Ruminski, J.L. Kiplinger, Inorg. Chem. 29 (1990) 4581.
[5] C.R. Arana, H.D. Abruña, Inorg. Chem. 32 (1993) 194.
[6] L.M. Vogler, B. Scott, K.J. Brewer, Inorg. Chem. 32 (1993) 898.
[7] M. Graf, B. Greaves, H. Stoeckli-Evans, Inorg. Chim. Acta 204 (1993) 239.
[8] L.M. Vogler, K.J. Brewer, Inorg. Chem. 35 (1996) 818.
[9] M. Graf, H. Stoeckli-Evans, A. Escuer, R. Vicente, Inorg. Chim. Acta 257 (1997) 89.
[10] J.-D. Lee, L.M. Vrana, E.R. Bullock, K.J. Brewer, Inorg. Chem. 37 (1998) 3575.
[11] C.M. Hartshorn, N. Daire, V. Tondreau, B. Loeb, T.J. Meyer, P.S. White, Inorg. Chem. 38 (1999) 3200.
[12] W.M. Teles, N.L. Speziali, C.A.L. Filgueiras, Polyhedron 19 (2000) 739.
[13] X. Chen, F.J. Femia, J.W. Babich, J. Zubieta, Inorg. Chim. Acta 315 (2001) 66.
[14] J.K. Bera, C.S. Campos-Fernández, C. Rodolphe, K.R. Dunbar, Chem. Commun. (2002) 2536.
[15] C.J. Kuehl, R.E. da Re, B.L. Scott, D.E. Morris, K.D. John, Chem. Commun. (2003) 2336.
[16] J. Carranza, C. Brennan, J. Sletten, J.M. Clemente-Juan, F. Lloret, M. Julve, Inorg. Chem. 42 (2003) 8716.
[17] R. Lalrempuia, P. Govindaswamy, Y.A. Mozharivskyj, M.R. Kollipara, Polyhedron 23 (2004) 1069.
[18] S. Fantacci, F. de Angelis, J. Wang, S. Bernhard, A. Selloni, J. Am. Chem. Soc. 126 (2004) 9715.
[19] N. Chanda, B. Sarkar, S. Kar, J. Fiedler, W. Kaim, G.K. Lahiri, Inorg. Chem. 43 (2004) 5128.
[20] M. Maekawa, T. Minematsu, H. Konaka, K. Sugimoto, T. Kuroda-Sowa, Y. Suenaga, M. Munakata, Inorg. Chim. Acta 357 (2004) 3456.
[21] J. Carranza, J. Sletten, C. Brennan, F. Lloret, J. Cano, M. Julve, J. Chem. Soc., Dalton Trans. (2004) 3997.
[22] H. Hadadzadeh, A.R. Rezvani, G.P.A. Yap, R.J. Crutchley, Inorg. Chim. Acta 358 (2005) 1289.
[23] G.-Y. Hsu, C.-W. Chen, S.-C. Cheng, S.-H. Lin, H.-H. Wei, C.-J. Lee, Polyhedron 24 (2005) 487.
[24] R.S. Bitzer, C.A.L. Filgueiras, J.G.S. Lopes, P.S. Santos, M.H. Herbst, Transition Met. Chem. 30 (2005) 636.
[25] Selected references: (a) M.C. Aragoni, M. Arca, F.A. Devillanova, M.B. Hursthouse, S.L. Huth, F. Isaia, V. Lippolis, A. Mancini, H. Ogilvie, Inorg. Chem. Commun. 8 (2005) 79;
(b) C.W. Padgett, R.D. Walsh, G.W. Drake, T.W. Hanks, W.T. Pennington, Cryst. Growth Des. 5 (2005) 745.
[26] Selected references: (a) E. Burkholder, J. Zubieta, Inorg. Chim. Acta 357 (2004) 1229;
(b) E. Burkholder, V. Golub, C.J. O'Connor, J. Zubieta, Inorg. Chem. 43 (2004) 7014;
(c) E. Burkholder, J. Zubieta, Inorg. Chim. Acta 358 (2005) 116.
[27] R.S. Bitzer, W.M. Teles, A. Abras, J.D. Ardisson, C.A.L. Filgueiras, J. Braz. Chem. Soc. 16 (2005) 963.
[28] A. Vlček Jr., Coord. Chem. Rev. 230 (2002) 225, and references therein.
[29] W. Kaim, S. Kohlmann, Inorg. Chem. 25 (1986) 3306.
[30] E.S. Dodsworth, A.B.P. Lever, Inorg. Chem. 29 (1990) 499.
[31] J.v. Slageren, A. Klein, S. Záliš, D.J. Stufkens, Coord. Chem. Rev. 219–221 (2001) 937.
[32] Selected references: (a) K. Nakamoto, Infrared and Raman Spectra of Inorganic and Coordination Compounds, Wiley–Interscience, New York, 1997;
(b) R.S. Czernuszewicz, K. Nakamoto, D.P. Strommen, J. Am. Chem. Soc. 104 (1982) 1515;
(c) T.G. Spiro, R.S. Czernuszewicz, in: L. QueJr. (Ed.), Resonance Raman Spectroscopy in Physical Methods in Bioinorganic Chemistry: Spectroscopy and Magnetism, University Science Books, Sausalito, 2000.
[33] H.A. Goodwin, F. Lions, J. Am. Chem. Soc. 81 (1959) 6415.
[34] D.J. Darensbourg, R.L. Kump, Inorg. Chem. 17 (1978) 2680.
[35] JAGUAR 5.5, Schrödinger, L.L.C., Portland, OR, 1991–2003.
[36] A.D. Becke, J. Chem. Phys. 98 (1993) 5648.
[37] P.J. Hay, W.R. Wadt, J. Chem. Phys. 82 (1985) 299.